# Nanoscale investigation by TEM and STEM-EELS of the laser induced yellowing

Marie Godet, Véronique Vergès-Belmin, Nicolas Gauquelin, Mandana Saheb, Judith Monnier, Eric M. Leroy, Julie Bourgon, Johan Verbeeck, Christine Andraud

Nanoscale investigation by TEM and STEM-EELS of the laser induced yellowing

## Nanoscale investigation by TEM and STEM-EELS of the laser induced yellowing

Marie Godet [a,b,c,1], Véronique Vergès-Belmin[a], Nicolas Gauquelin[d], Mandana Saheb[e], Judith Monnier[f], Eric Leroy[f], Julie Bourgon[f], Johan Verbeeck[d], Christine Andraud[b]

[a] Laboratoire de Recherche des Monuments Historiques (CRC-LRMH USR 3224), 29 rue de Paris 77420 Champs-sur-Marne, France ; veronique.verges-belmin@culture.gouv.fr

[b] Centre de Recherche et Conservation des Collections (CRC-CRCC USR 3224), 36 rue Geoffroy-Saint-Hilaire – CP 21, 75005 Paris, France ; candraud@mnhn.fr

[c] SILLTEC, Domaine Technologique de Saclay, 4, rue René Razel, 91400 Saclay, France

[d] Electron microscopy for materials science (EMAT), University of Antwerp, Antwerpen, Belgium; nicolas.gauquelin@uantwerpen.be; jo.verbeeck@uantwerpen.be

[e] Laboratoire Interdisciplinaire des Systèmes Atmosphériques (LISA), UMR CNRS 7583, Université Paris-Est Créteil and Université Paris-Diderot, Institut Pierre Simon Laplace, Créteil, France ; mandana.saheb@lisa.u-pec.fr;

[f] Université Paris Est, ICMPE (UMR 7182), CNRS, UPEC, F-94320 Thiais, France ; monnier@icmpe.cnrs.fr; eric.leroy@u-pec.fr; bourgon@icmpe.cnrs.fr;

*corresponding author: msgodet@gmail.com (marie.godet@upmc.fr); +33660338427; present address: IMPMC, 4 place jussieu 75005 Paris, France

**Declarations of interest: none**

## Graphical abstract (color)

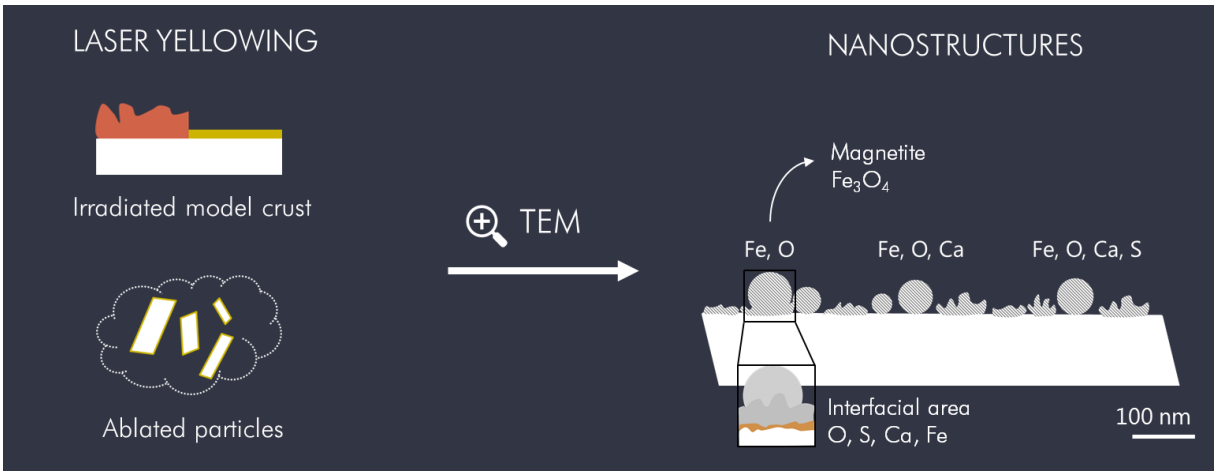


## Highlights:

- Laser yellowing is linked to the appearance of iron-rich nanostructures
- The iron-rich nanostructures are crystallized
- Two morphologies are observed : nano-spheres and nano-residues
- The nanostructures always contain O and Fe and occasionally Ca and S

- Magnetite $Fe_3O_4$ is detected at the nanoscale


## Abstract

Nd:YAG QS laser cleaning of soiled stone at 1064 nm can sometimes result in a more yellow appearance compared to other cleaning techniques. Especially in France, this yellowing effect is still considered as a major aesthetic issue by the architects and conservators. One explanation states that the yellowing is linked to the formation of iron-rich nanophase(s) through the laser beam interaction with black crusts that would re-deposit on the cleaned substrate after irradiation. To characterize these nanophases, a model crust containing hematite was elaborated and laser irradiated using a Nd-YAG QS laser. The color of the sample shifted instantaneously from red to a bright yellow and numerous particles were ablated in a visible smoke. Transmission electron microscopy (TEM) was used to examine the morphology and the crystallinity of the neo-formed compounds, both on the surface of the samples and in the ablated materials. In addition, an investigation of the chemical and structural properties of the nanophases was conducted by X-ray dispersive energy (EDX) and electron energy loss (EELS) spectroscopies. It was found that both the surface of the sample and the ablated materials are covered by crystallized nano-spheres and nano-residues, all containing iron and oxygen, sometimes along with calcium and sulfur. In particular an interfacial area containing the four elements was evidenced between some nanostructures and the substrate. Magnetite $Fe_3O_4$ was also identified at the nanoscale. This study demonstrates that the laser yellowing of a model crust is linked to the presence of iron-rich nanophases including $Ca_xFe_yS_zO_\delta$ nanostructures and magnetite $Fe_3O_4$ at the surface after irradiation.



**Keywords:** laser cleaning, yellowing, nanostructures, iron, TEM, EELS


## 1. Introduction

Nd-YAG Q-Switched laser devices operating at 1064 nm were considered in the 1990s as the most promising tool to eliminate indurated black gypsum crusts from stone sculptures (Cooper, 1998). However, the spreading of this laser technology was undermined as a consequence of the yellow hue it occasionally conveys to the cleaned surfaces (Vergès-Belmin and Dignard, 2003). This yellowing effect was, and still is considered as a major issue by conservators and architects: it has raised a strong esthetic controversy in the 2000s especially in France where the market of laser cleaning of built heritage has almost totally disappeared nowadays despite its high efficiency (Vergès-Belmin et al., 2014). To enable the laser technique to regain a place in restorers' toolbox, this yellowing needs to be avoided. The first step is therefore to understand the origin of this phenomenon; therefore, several studies have been conducted by laboratories since the 2000s. A currently admitted hypothesis states that the yellowing is linked to the creation of neo-formed compounds through the laser interaction with black crusts. Those compounds would redeposit instantaneously on the cleaned substrate upon irradiation (Pouli et al., 2012; De Oliveira et al., 2016a). To verify this hypothesis,

most studies have been conducted on model crust samples elaborated by mixing synthetic gypsum $CaSO_4.2H_2O$ and 1064 nm absorbing compounds present in black crusts such as iron oxides (hematite $\alpha$-$Fe_2O_3$) and carbonaceous compounds (graphite, carbon black) (Klein *et al.*, 2001; Zhang *et al.*, 2007; De Oliveira *et al.*, 2016a). These authors applied the mixture on white marble or plaster substrates. The model crusts were irradiated using a Nd-YAG QS (1064 nm) laser and the color of the samples immediately turned to a bright yellow while numerous particles were ejected in a visible smoke.

Some neo-formed compounds have been observed using scanning electron microscopy (SEM) at the surface of the samples after irradiation (Klein et al., 2001; De Oliveira et al., 2016a). However, the chemical and structural nature of the compounds turned out to be very complex to elucidate, due to the very low amount of matter available and to the nanometric size of the neoformed material. Investigating such deposits has thus required the use of sensitive analytical probes specific to nanometer-sized objects.

A few studies have focused on the ablated particulate materials and have shown that they also contribute to the yellowing effect (Vergès-Belmin and Dignard, 2003; Godet et al., 2016, 2017). In particular, nanostructures containing iron (Fe), oxygen (O) and often calcium (Ca) have been evidenced on the surface of some ablated gypsum particles using optical, scanning and transmission electron microscopies (SEM and TEM) (Godet et al., 2016). Traces of sulfur (S) were also detected, but its detection was difficult to ascertain at the nanoscale. Besides, as the analysed nanostructures were located on the surface of ablated gypsum particles, part of the Ca and S detected by analytical SEM and TEM might have originated from the gypsum substrate ($CaSO_4.2H_20$). In addition, the study did not provide any analysis of the irradiated yellow substrate, leaving some uncertainties on the nature of the nanostructure present on the yellow substrate surface after irradiation.

The present study aims at filling this gap and at deepening the characterization of the neo-formed compounds responsible for the yellowing of a model crust containing gypsum and hematite. To this purpose, the development of a multi-techniques nanoscale characterization is necessary. A transmission electron microscope (TEM) has been used to examine the morphology of the nanostructures, both in the ablated materials and on the surface of the sample. The compounds crystallinity has been studied by selected-area electron diffraction (SAED). In addition, scanning transmission electron microscopy imaging (STEM) coupled to energy dispersive X-ray (EDX) and electron energy-loss (EELS) spectroscopies have been used to determine the chemical composition of the neo-formed phases. Finally, the nature of some nanophases have been identified using electron energy-loss near edge structure (ELNES) spectroscopy coupled to high angle annular dark field imaging (HAADF) by comparison with references.

## 2. Materials and methods

### 2.1 Model crust preparation and laser irradiation

A model crust containing 30 $_{wt}$% hematite (ALDRICH, 99%) was elaborated following the experimental procedure described in De Oliveira et al. (2016b): a white gypsum plate was synthesized by hydration of a powder of pure calcium sulfate hemihydrate (ALDRICH, 97%) in distilled water. While the plate was still wet, a mixture of the same calcium sulfate hemihydrate and red hematite $\alpha$-$Fe_2O_3$ (ALDRICH, 99%) powders (70:30 $_{wt}$%) was sprinkled over the plate through a coarse-meshed sieve (about 1 mm). The remaining water in the plate was absorbed by hemihydrate powder thus allowing the crystallization of gypsum as a crust entrapping particles of hematite and with a microstructure very similar to that of a natural black gypsum crust. The crust was left to dry for 24 hours.

The model crust was then irradiated using a Nd:YAG Q-switched laser from Thomson BM Industries. The laser, operating at a wavelength of 1064 nm, produces discrete pulses of laser energy up to 0.4 J, with a pulse duration of 15 ns. The pulses were delivered using an articulated mirrored arm and a hand-piece equipped with a 70 cm focal length convergent lens. The fluence was slowly increased from 0.4 to 0.6 J.cm$^{-2}$ during the cleaning process. The pulse frequency was 10 Hz and the sample was irradiated at a rate of 3 min.cm$^{-2}$; signifying that about 1800 pulses are used to clean the samples. The surface of the sample was sprayed with water prior to irradiation. During the irradiation, the ablated particulate material was collected on a clean glass slide (76x26 mm$^2$) put vertically aside the sample at a distance of about 1 cm. The slide was then stored in an airtight box to prevent contamination. Two types of samples were thus finally available for examination: the irradiated model crust and the ablated particles.

### 2.2 Transmission Electron Microscopy analyses

TEM analysis was first performed at 200 kV with a FEG Tecnai F20 equipped with a STEM device and with an EDAX R-TEM Sapphire Si(Li) EDX detector. The EDX capability coupled to the TIA ES Vision software (FEI inc.) were used to determine the chemical composition of the compounds of interest. A sample was prepared by gently scraping the surface of the irradiated crust substrate under a binocular magnifier. The resulting yellow powder was then diluted in ethanol and the whole is placed three minutes in an ultrasound bath. One drop of the suspension was finally deposited on a copper grid covered by a holey amorphous carbon film. As for the ablated particles, a sample was prepared by rubbing gently the surface of the glass slide with the same type of copper grid.

In a second step, STEM-HAADF imaging and STEM-EELS experiments were performed at 300 kV using a double aberration corrected FEI Titan$^3$ QU-Ant-EM microscope equipped with a GIF Quantum spectrometer.

For this experiment, two FIB cuts were prepared with a FEI Hélios NanoLab 650 Dual beam microscope: one from the irradiated surface and one from an ablated yellow gypsum particle. During the FIB preparation, a few nanometres thick layer of carbon (C) was first applied on the samples to make them conductive. A few micrometres thick layer of platinum (Pt) was

then coated on the surface to protect the samples. Afterwards the FIB cuts were carved and thinned using a gallium (Ga) ions beam.

For EELS analyses, spectrum-images were acquired with a spatial resolution varying between 0.5 Å and 1 Å, and with an energy resolution of approximately 1 eV. Digital Micrograph software (Gatan inc.) and EELSTools script (Mitchell and Schaffer, 2005) were used to process raw EELS data. Edge intensity maps were extracted from the spectrum-images to spatially localize the different chemical elements. EELS spectra were also extracted and their background was subtracted to study the general shape of the various ionization edges. A monochromator was used to study the fine structures of the Fe L and O K ionization edges with a resolution up to 0.3 eV (ELNES).

All the TEM observations were made at liquid nitrogen temperature (-172°C) with a cooling sample holder in order to limit the gypsum degradation during analysis.

## 3. Results

### 3.1 Morphology and cristallinity

For both types of samples, micro-particles of gypsum in the form of rods and platelets are observed. Two types of nanostructures are detected at their surface (Figure 1):

- Rounded or spherical nanoparticles (nano-spheres), whose diameter ranges from 20 nm to a few hundred nanometres.
- Irregular nano-residues in the form of stacks of particles measuring individually less than 10 nm. The stacks are generally smaller than 50 nm.

These two types of nanostructures are also observed isolated on the holey carbon film (Figure 1b., d.). The nano-spheres are often covered by irregular nano-residues.

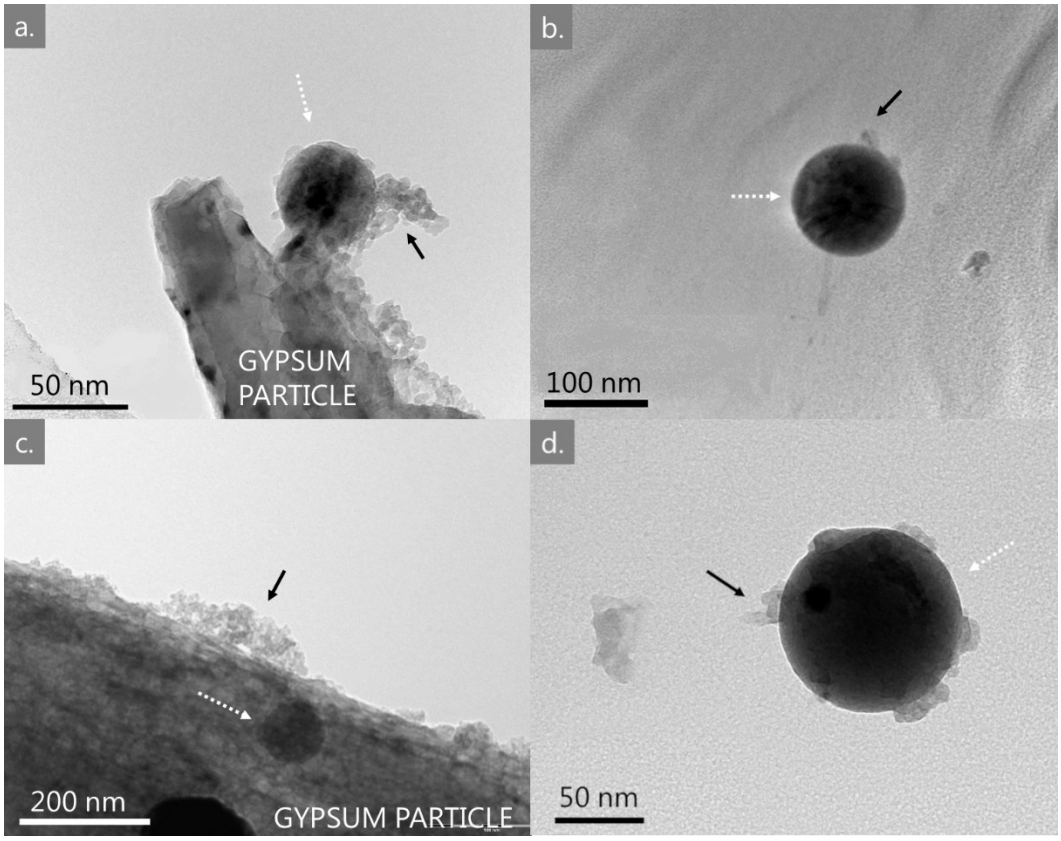


Figure 1: Nanostructures observed on the ablated particles (a., b.) and on the irradiated substrate (c., d.); left = at the surface of a gypsum particle; right = isolated on the carbon film (TEM-BF images); Legend: white arrows = nano-spheres; black arrows = irregular nano-residues.

Examination of the FIB lamellas confirms the previous observations (Figure 2). STEM-HAADF imaging of the FIB cut prepared from the ablated particle shows two nano-spheres, one whose diameter is approximately 50 nm, will be called *small nano-sphere* and one with a diameter above 100 nm detached from the surface which will be called *big nano-sphere*. Irregular nano-residues with a thickness lower than 50 nm are also observed on the gypsum substrate surface.

Examination of the second FIB cut prepared from the irradiated surface reveals the presence of a *rounded nanoparticle* which larger size is approximately 50 nm and some nano-residues forming a thin (less than 20 nm) and continuous layer at the surface of the gypsum substrate.

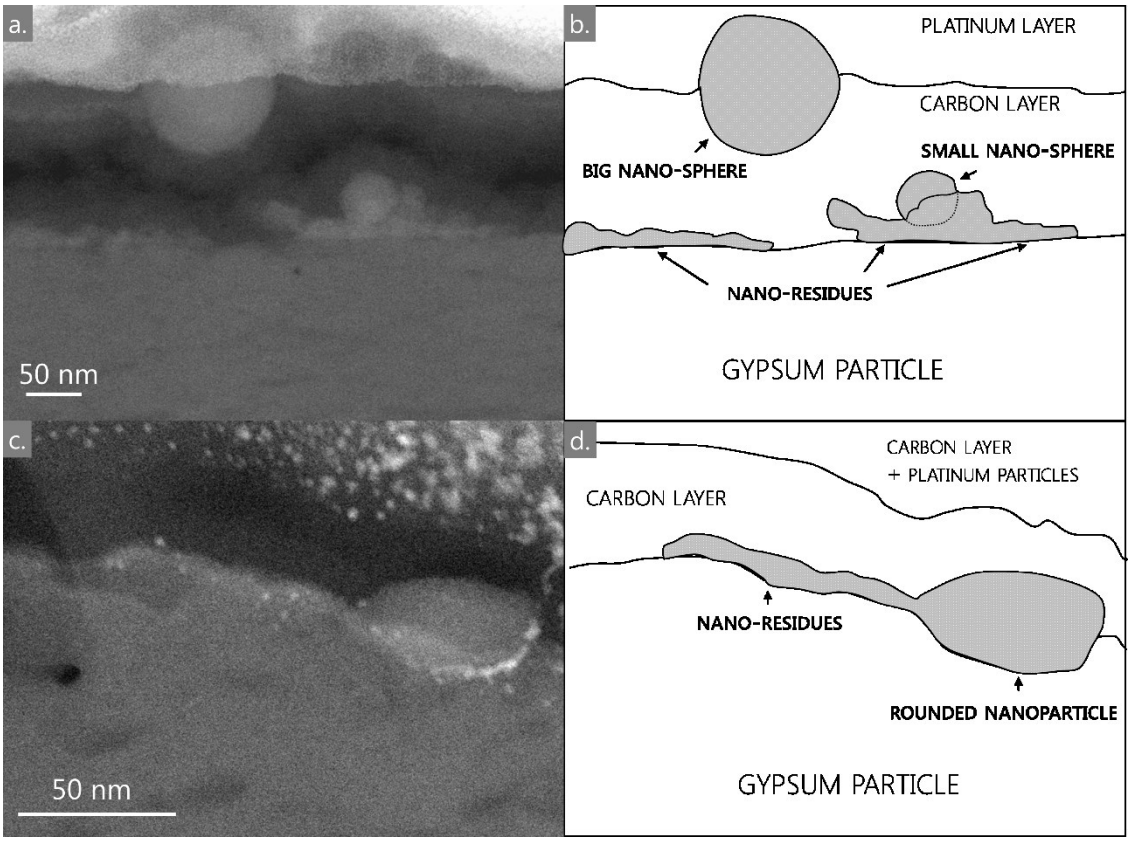


Figure 2: FIB cut at the surface of one ablated gypsum particle (a., b.) and of the irradiated substrate (c., d.); left = STEM-HAADF image; right = explicative drawing.

SAED shows networks of spots indicating that the nanostructures are crystalline (Figure 3). Most of the nano-spheres are single crystalline (Figure 3c). Diffraction patterns obtained on the nano-residues covering the gypsum particle show some single-crystal lattices entangled together corresponding to the simultaneous diffraction of several compounds or else to compounds with different orientations (Figure 3d).

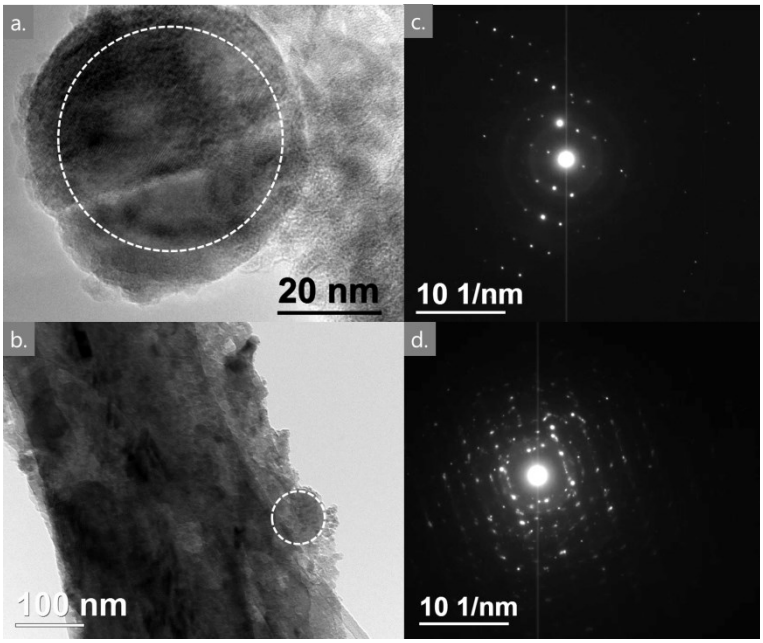


Figure 3: Electron diffraction patterns (SAED) obtained on the nanostructures ; a. nano-sphere (TEM-BF image) ; b. nanostructures at the surface of a gypsum rod (TEM-BF image); c. et d. corresponding diffraction patterns (acquired on the dotted white circle area).

### 3.2 Chemical and structural investigation

To perform the elemental analysis, quantitative STEM-EDX was coupled to STEM-EELS – a more qualitative but highly sensitive technique. For both irradiated substrate and ablated particles samples the chemical analysis leads to the same results.

Three types of chemical composition, O-Fe, O-Ca-Fe, or O-S-Ca-Fe can be found in various proportions which bear no relation to the morphology of the nanostructures (sphere or residues). In other words, both nano-sphere and nano-residues may contain O, Fe, (Ca), (S) in variable amounts.

In all cases, O and Fe are the main elements (Figure 4, Table 1). The Ca amount is very variable up to more than 20 wt% whereas S is always present in trace amounts (<2 wt%). S is however easily detected by EELS due to the high analytical sensitivity of this technique (Figure 5) (Grieten et al., 2017).

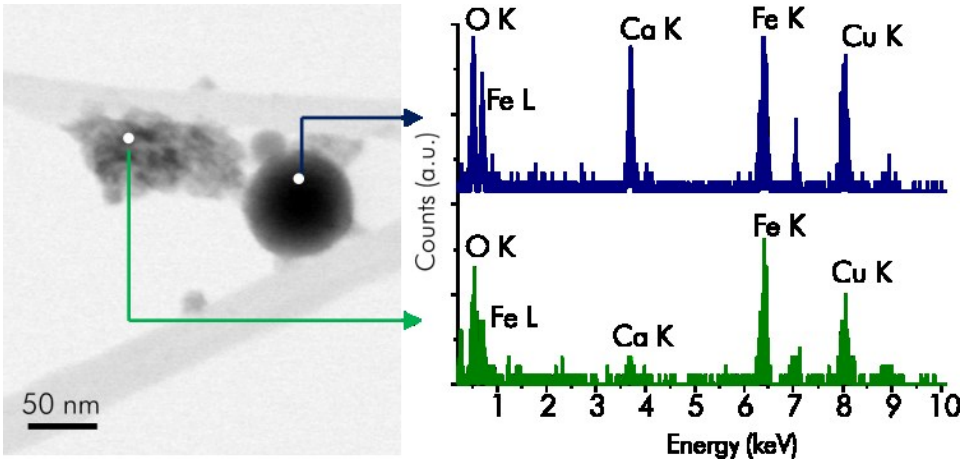


Figure 4: STEM-EDX analysis of isolated nanostructures (ablated particles); left = STEM-BF image, the light gray lines correspond to the holey carbon support ; right = corresponding EDX spectra (copper (Cu) originates from the copper grid).

Table 1: Normalized chemical composition extracted from the Figure 4 spectra (in weight %).

| $\%_{wt}$ | O | Ca | Fe |
|---|---|---|---|
| Nano-sphere | 37.4 | 19.3 | 42.8 |
| σ | 3.2 | 1.6 | 2.7 |
| Nano-residues | 49.8 | 2.9 | 47.3 |
| σ | 5.3 | 1.6 | 4.0 |

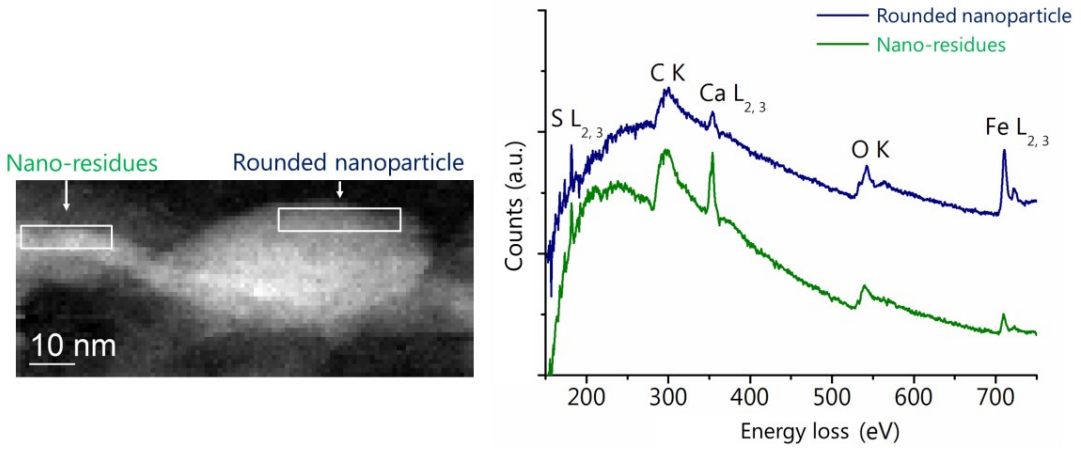


Figure 5: STEM-EELS analysis of nanostructures (irradiated substrate); left = spectrum-image (1 nm/pixel); right = EELS spectra extracted from the indicated area on the spectrum-image, the C detected originates from the carbon layer applied during the FIB preparation.

Elemental spatial distribution studied by extracting EELS edge intensity maps from a spectrum-image for the Ca $L_{2,3}$, S $L_{2,3}$, O K and Fe $L_{2,3}$ edges is presented in Figure 6 for the *small nano-sphere*. The different maps show that the *small nano-sphere* and the adjacent irregular nano-residues are mainly composed of O and Fe whereas the gypsum substrate contains, as expected, O, S and Ca. It is worth noting that Ca and S seem to be present in some sparse area of the nanostructures (dispersed yellow and red pixels on the figure 6c). In particular a thin interfacial layer (1-2 nanometres thick) containing the four elements O, S, Ca and Fe, seems to be present between the nanostructures and the substrate.

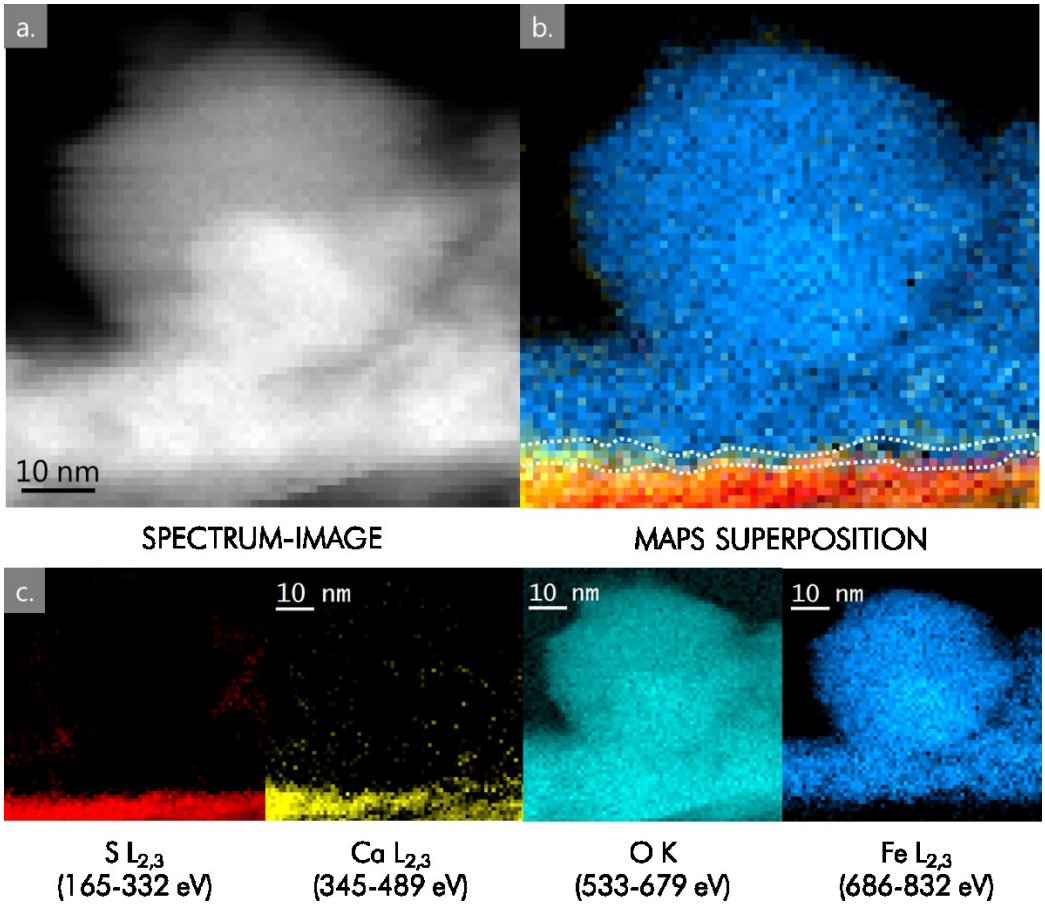


Figure 6: EELS analyses of the small nano-sphere and the adjacent nano-residues; a. spectrum-image (0.5 Å/pixel); b. maps superposition; c. edge intensity maps extracted from a.; the interfacial area is delineated by broken lines on b. (COLOR)

EELS edges spectra are extracted from the different regions of interest with a resolution of approximately 1 eV (Figure 7). O K edges obtained from the *small nano-sphere* and the nano-residues are showing a pre-peak and are different from those obtained on the interfacial area and on the gypsum substrate which only present a weak shoulder. The O thus seems to have two types of chemical environment and bonding. Regarding the other elements, S, Ca and Fe $L_{2,3}$ edges present similar fine structures in the different regions. In particular the Fe L edges are all shapeless without any discernible pre-peak (a typical fine structure observed for pure

trivalent iron oxides (Chen et al., 2009). These results indicate that the three elements configuration (valence and local geometry) are similar in the different analysed area and that Fe is probably not purely trivalent, meaning that $Fe^{(III)}$ and $Fe^{(II)}$ are both present.

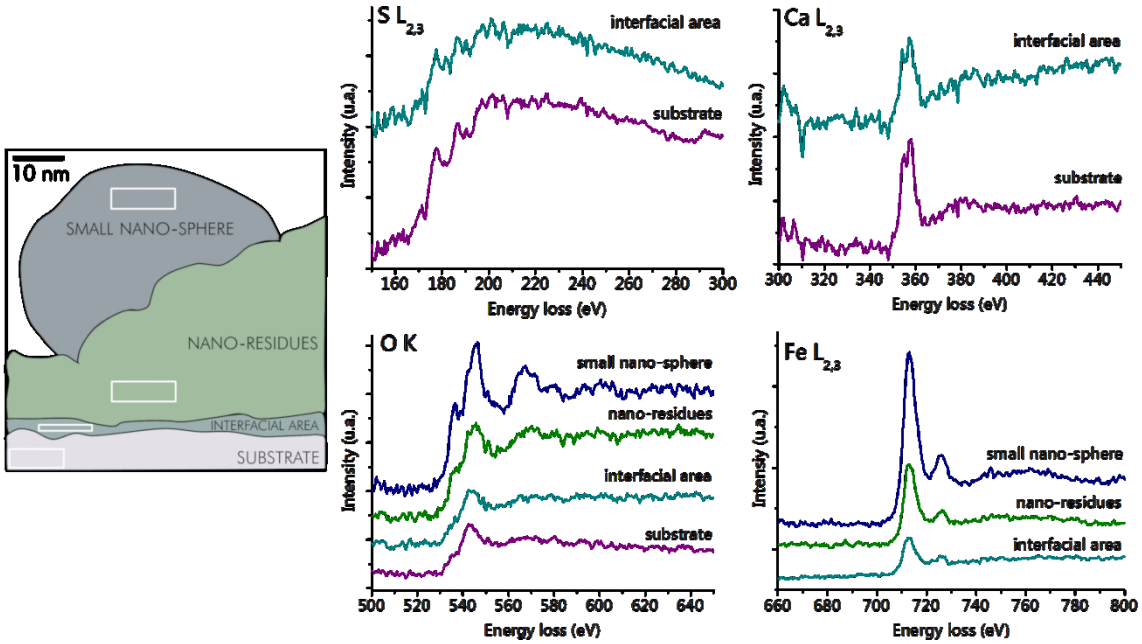


Figure 7: EELS analysis of different area around the small nano-sphere; left = schematic drawing with analyses localization (white rectangle); right = EELS edges obtained on the different regions of interest. (COLOR)

In order to clarify the nature of the nano-spheres, monochromated EELS analysis has been conducted with an optimized energy resolution of 0.3 eV (ELNES). Figure 8 shows the results for the *big nano-sphere* (only containing O and Fe). Analysis of the Fe L and O K edges reveals the same fine structures as magnetite $Fe^{(II, III)}{}_3O_4$ (Almeida et al., 2014). Indeed, the Fe $L_2$ edge seems to be the sum of three different contributions with a local maximum around 722 eV which is typically observed for mixed valence compounds like magnetite (Figure 8b). Furthermore, the $L_3$ edge is almost shapeless which is often interpreted as the contributions of iron in both octahedral and tetrahedral sites (Gloter et al., 2004), both present in magnetite (Table 1). As for the O K edge, it is typical of those observed for pure magnetite, revealing a single pre-peak with a shoulder on the high-energy side followed by a broad edge at higher energy (Figure 8c) (Chen et al., 2009). Therefore we can ascertain that the *big nano-sphere* is a nanoparticle of magnetite.

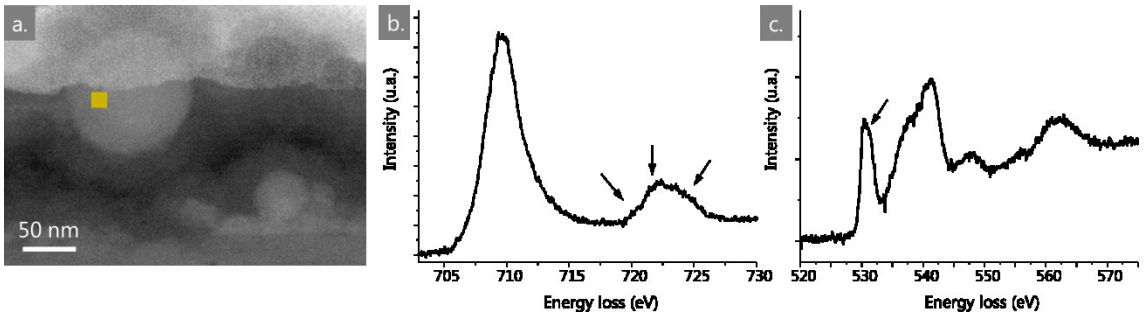


Figure 8: ELNES spectra obtained on the big nano-sphere (0.3 eV); a. STEM-HAADF image with the analyzed area marked; b. Fe $L_{2,3}$ edge; c. O K edge ; black arrows indicate the fine structure features used for identification.

## 4. Discussion

A study previously conducted by Godet et al. (2016) on a model crust containing hematite α-$Fe_2O_3$ has shown that nanostructures are present on the ablated particles after laser irradiation. The present study completes these preliminary results as it demonstrates that these nanostructures are present both on the ablated particles and on the irradiated gypsum substrate. Besides, it shows that the nanostructures are crystallized in the form of spheres and irregular residues and contain O and Fe, often accompanied with Ca and S in various proportions.

The nanostructures containing only O and Fe crystallize in the form of iron oxides (or iron oxi-hydroxides) which have been extensively described in the literature (Cornell and Schwertmann, 2003). Table 2 displays the valence and geometry of Fe atoms in the most common iron oxi-(hydroxi)des.

Table 2: Valence and geometry of Fe atoms in some iron oxi-(hydroxi)des (Cornell and Schwertmann, 2003)

| Name | Formula | Iron valence | Iron geometry |
|---|---|---|---|
| Hematite | α-$Fe_2O_3$ | 3 | octahedral |
| Maghemite | γ-$Fe_2O_3$ | 3 | 2/3 octahedral<br>1/3 tetrahedral |
| Goethite | α-FeOOH | 3 | octahedral |
| Lepidocrocite | γ-FeOOH | 3 | octahedral |
| Ferrihydrite | $Fe_5HO_8.4H_2O$ | 3 | octahedral |
| Magnetite | $Fe_3O_4$ | 2 and 3 | 2/3 octahedral<br>1/3 tetrahedral |

In this study magnetite $Fe^{(II, III)}{}_3O_4$ has been identified at the nanoscale. Magnetite is a well-known product of the Nd:YAG (1064 nm) laser irradiation of pure hematite (da Costa, 2002;

Sanz et al., 2013). It has also been detected after irradiation of model crusts in some previous studies but only at the macro- (Gracia et al., 2005) or microscale (De Oliveira, 2014). To our knowledge it is the first time that magnetite has been detected at the nanoscale after irradiation of a model crust. However, as magnetite is black at the macro and microscale, the question of its contribution to the yellowing has immediately raised. A modelling of the color produced by a system composed of magnetite nanoparticles dispersed on a white substrate has been carried out in Godet (2017). This modelling, based on 4-flux calculations, described in details in Genty-Vincent et al. (2017), has shown that the color produced by such a system is ochre beige, indicating therefore that the presence of nano-spheres of magnetite on the gypsum substrate surface can contribute to the yellowing effect. Several others iron oxides such as goethite $\alpha$-FeOOH, lepidocrocite $\gamma$-FeOOH or maghemite $\gamma$-$Fe_2O_3$ have yellow-orange tonalities but none of these compounds have been identified in the present investigation. A diffuse reflectance study previously conducted by De Oliveira et al. (2016b) on a crust sample reconstituted from some powdery soiling dust has shown that the yellow color obtained after laser irradiation is linked to an optical spectrum similar to the one of goethite $\alpha$-FeOOH. As different minerals can have the same optical spectrum, further structural studies are however still needed to ascertain this hypothesis.

Aside from iron oxy-hydroxides, crystalline nanostructures containing O, Fe and Ca have also been detected in the present study. These ternary compounds are stable at room temperature and ambient pressure under the form of calcium ferrites $Ca_xFe_yO_z$, solid solutions containing iron and calcium oxides ($Fe^{2+}$, $Fe^{3+}$, $Ca^{2+}$ ) ($O^{2-}$) or various complex oxides such as spinels $(Fe^{2+},Fe^{3+})^{T}[Fe^{2+}, Fe^{3+},Ca^{2+}]_2^{O}O_4^{2-}$ (Gerardin et al., 1989; Hidayat et al., 2016). Some of these nanostructures also include S in trace amounts, in particular at the interface between the nanostructures and the gypsum substrate. To our knowledge no crystallised compounds containing only these four elements have been described in literature. However, as the S is always detected in low quantities, we can suppose that these nanostructures have similar structures as those of O-Ca-Fe compounds incorporating additional S atoms.

The question now rising is: what elements are responsible of the yellow color? A common feature of the neo-formed compounds is that they all contain Fe. As Fe is a well-known coloring agent in many yellow minerals and pigments (Burns, 1993), this element is probably responsible of the yellow hue obtained after irradiation. Further studies on the structure and the optical properties of the Fe-rich compounds would be useful to determine which type(s) of the neo-formed compounds identified in this study is (are) responsible of the yellow color.

## 5. Conclusion

TEM analyses have revealed that the yellowing resulting from the laser ablation of a model crust containing hematite is linked to the formation of crystallized nanostructures (nano-spheres and nano-residues) containing O and Fe, sometimes along with Ca and S. Among the neo-formed phases, magnetite $Fe_3O_4$ was identified for the first time at a nanoscale on such model crusts.

This study attests that the laser yellowing – a chromatic modification observed at the macroscale – is intimately linked with matter transformation at the nanoscale. It also reveals the potential of using TEM and associated techniques (diffraction, EDX, EELS) - to study complex and heterogeneous nanostructured materials linked to cultural heritage preservation.

## 6. Acknowledgements

The authors wish to thank Valérie Lalanne for the sample preparation for TEM and Stijn Van den Broeck for the FIB cut elaboration. The research leading to these results has received funding from the European Union Seventh Framework Programme under Grant Agreement 312483 - ESTEEM2 (Integrated Infrastructure Initiative–I3).

## 7. References

Almeida, T.P., Kasama, T., Muxworthy, A.R., Williams, W., Nagy, L., Hansen, T.W., Brown, P.D., Dunin-Borkowski, R.E., 2014. Visualized effect of oxidation on magnetic recording fidelity in pseudo-single-domain magnetite particles. Nature Communications 5, 5154. https://doi.org/10.1038/ncomms6154

Burns, R.G., 1993. Mineralogical applications of crystal field theory. Cambridge University Press, Cambridge.

Chen, S.-Y., Gloter, A., Zobelli, A., Wang, L., Chen, C.-H., Colliex, C., 2009. Electron energy loss spectroscopy and ab initio investigation of iron oxide nanomaterials grown by a hydrothermal process. Physical Review B 79. https://doi.org/10.1103/PhysRevB.79.104103

Cooper, M., 1998. Laser Cleaning in Conservation: an introduction. Butterworth-Heinemann, Oxford.

Cornell, R.M., Schwertmann, U., 2003. The Iron Oxides. Wiley-VCH Verlag GmbH & Co. KGaA, Weinheim, FRG. https://doi.org/10.1002/3527602097

da Costa, A.., 2002. Ultra-fast dehydration and reduction of iron oxides by infrared pulsed radiation. Scripta Materialia 47, 327–330. https://doi.org/10.1016/S1359-6462(02)00150-1

De Oliveira, C., 2014. JAPILA: Jaunissement de la pierre par laser, mécanismes et remèdes (PNRCC).

De Oliveira, C., Vergès-Belmin, V., Demaille, D., Bromblet, P., 2016a. Lamp black and hematite contribution to laser yellowing: A study on technical gypsum samples. Studies in Conservation 61, 136–145. https://doi.org/10.1179/2047058415Y.0000000003

De Oliveira, C., Vergès-Belmin, V., Lafait, J., Swider, M., Andraud, C., Tournié, A., Galoisy, L., 2016b. Contribution of goethite to laser-induced stone yellowing. Applied Physics A 122, 467. https://doi.org/10.1007/s00339-016-9818-z

Genty-Vincent, A., Van Song, T.P., Andraud, C., Menu, M., 2017. Four-flux model of the light scattering in porous varnish and paint layers: towards understanding the visual appearance of altered blanched easel oil paintings. Applied Physics A 123. https://doi.org/10.1007/s00339-017-1092-1

Gerardin, R., Bonazebi, A., Millon, E., Brice, J.F., Evrard, O., Sanchez, J.P., 1989. Etude des magnétites dopées à la chaux : substitution du fer par le calcium en site tétraédrique. Journal of Solid State Chemistry 78, 154–163.

Gloter, A., Zbinden, M., Guyot, F., Gaill, F., Colliex, C., 2004. TEM-EELS study of natural ferrihydrite from geological–biological interactions in hydrothermal systems. Earth and Planetary Science Letters 222, 947–957. https://doi.org/10.1016/j.epsl.2004.03.040

Godet, M., 2017. Jaunissement de la pierre par laser : origines et remèdes (Thèse en science des matériaux). Muséum National d'Histoire Naturelle, Paris.

Godet, M., Vergès-Belmin, V., Andraud, C., Saheb, M., Monnier, J., Leroy, E., Bourgon, J., 2016. Laser yellowing of hematite-gypsum mixtures: a multi scale characterization, in: Science and Art: A Future for Stone. Presented at the 13th International Congress on the Deterioration and Conservation of Stone, John Hughes & Howind Torsten, Paisley, pp. 785–792.

Godet, M., Vergès-Belmin, V., Andraud, C., Saheb, M., Monnier, J., Leroy, E., Bourgon, J., Binet, L., 2017. Laser yellowing effect: study of the nanophases created by laser irradiation of synthetic black crusts using transmission electron microscopy (TEM) and electron paramagnetic resonance (EPR) spectroscopy, in: Proceeding of the LACONA 11 Congress. Presented at the LACONA 11, P. Targowski et al., Krakow, pp. 63–76. https://doi.org/10.12775/3875-4.04

Gracia, M., Gaviño, M., Vergès-Belmin, V., Hermosin, B., Nowik, W., Sáiz-Jiménez, C., 2005. Mössbauer and XRD Study of the Effect of Nd:YAG-1064 nm Laser Irradiation on Hematite Present in Model Samples, in: Dickmann, K., Fotakis, C., Asmus, J.F. (Eds.), LACONA V. Springer-Verlag, Berlin/Heidelberg, pp. 341–346.

Grieten, E., Schalm, O., Tack, P., Bauters, S., Storme, P., Gauquelin, N., Caen, J., Patelli, A., Vincze, L., Schryvers, D., 2017. Reclaiming the image of daguerreotypes: Characterization of the corroded surface before and after atmospheric plasma treatment. Journal of Cultural Heritage 28, 56–64. https://doi.org/10.1016/j.culher.2017.05.008

Hidayat, T., Shishin, D., Decterov, S.A., Jak, E., 2016. Thermodynamic Optimization of the Ca-Fe-O System. Metallurgical and Materials Transactions B 47, 256–281. https://doi.org/10.1007/s11663-015-0501-0

Klein, S., Fekrsanati, F., Hildenhagen, J., Dickmann, K., Uphoff, H., Marakis, Y., Zafiropulos, V., 2001. Discoloration of marble during laser cleaning by Nd:YAG laser wavelengths. Applied Surface Science 171, 242–251.

Mitchell, D.R.G., Schaffer, B., 2005. Scripting customised microscopy tools for Digital Micrograph. Ultramicroscopy 103, 319–332.

Pouli, P., Oujja, M., Castillejo, M., 2012. Practical issues in laser cleaning of stone and painted artefacts: optimisation procedures and side effects. Applied Physics A 106, 447–464. https://doi.org/10.1007/s00339-011-6696-2

Sanz, M., Oujja, M., Rebollar, E., Marco, J.F., de la Figuera, J., Monti, M., Bollero, A., Camarero, J., Pedrosa, F.J., García-Hernández, M., Castillejo, M., 2013. Stoichiometric magnetite grown by infrared nanosecond pulsed laser deposition. Applied Surface Science 282, 642–651. https://doi.org/10.1016/j.apsusc.2013.06.026

Vergès-Belmin, V., De Oliveira, C., Rolland, O., 2014. Investigations on yellowing as an effect of laser cleaning at Chartres Cathedral, France, in: ICOM-CC 17th Triennial Conference Preprints. Presented at the ICOM-CC 17th Triennial Conference, J. Bridgland, Melbourne.

Vergès-Belmin, V., Dignard, C., 2003. Laser yellowing: myth or reality? Journal of Cultural Heritage 4, 238–244.

# Figure captions

Figure 1: Nanostructures observed on the ablated particles (a., b.) and on the irradiated substrate (c., d.); left = at the surface of a gypsum particle; right = isolated on the carbon film (TEM-BF images); Legend: white arrow = nano-spheres; black arrow = irregular nano-residues.

Figure 2: FIB cut at the surface of one ablated gypsum particle (a., b.) and of the irradiated substrate (c., d.); left = STEM-HAADF image; right = explicative drawing.

Figure 3: Electron diffraction patterns (SAED) obtained on the nanostructures; a. nano-sphere (TEM-BF image) ; b. nanostructures at the surface of a gypsum rod (TEM-BF image); c. et d. corresponding diffraction patterns (acquired on the dotted white circle area).

Figure 4: STEM-EDX analysis of isolated nanostructures (ablated particles); left = STEM-BF image, the light gray lines correspond to the holey carbon support; right = corresponding EDX spectra (copper (Cu) originates from the copper grid)

Figure 5: STEM-EELS analysis of nanostructures (irradiated substrate); left = spectrum-image (1 nm/pixel); right = EELS spectra extracted from the indicated area on the spectrum-image, the C detected originates from the carbon layer applied during the FIB preparation.

Figure 6: EELS analyses of the small nano-sphere and the adjacent nano-residues; a. spectrum-image (0.5 Å/pixel); b. maps superposition; c. edge intensity maps extracted from a.; the interfacial area is delineated by broken lines on b.

Figure 7: EELS analysis of different area around the small nano-sphere; left = schematic drawing with analyses localization (white rectangle); right = EELS edges obtained on the different regions of interest.

Figure 8: ELNES spectra obtained on the big nano-sphere (0.3 eV); a. STEM-HAADF image with analysis localization; b. Fe $L_{2,3}$ edge; c. O K edge ; black arrows indicate the fine structure used for identification.

# Table captions

Table 1: Normalized chemical composition extracted from the Figure 4 spectra (in weight %).

Table 2: Valence and geometry of Fe atoms in some iron oxi-hydroxides (Cornell & Schwertmann, 2003).